Electronic Supplementary Material (ESI) for Journal of Materials Chemistry A.

Supporting Information

Valorization of lignin waste: High electrochemical capacitance of Lignin-derived carbons in aqueous and ionic liquid electrolytes

Wantana Sangchoom, Darren Walsh and Robert Mokaya*

University of Nottingham, University Park, Nottingham NG7 2RD, U. K.

E-mail: r.mokaya@nottingham.ac.uk (R. Mokaya)

Table S1. Elemental composition (%) and H/C ratio of lignin-derived activated carbons

Sample	Elemental composition (%)			H/C ratio	O/C ratio
	C	H	O		
LAC600:2	67.8	1.36	30.84	0.02	0.34
LAC700:2	83.3	0.50	16.20	0.006	0.15
LAC800:2	85.9	0.35	13.75	0.004	0.12
LAC600:4	75.3	1.33	23.37	0.018	0.23
LAC700:4	78.3	0.52	21.18	0.0066	0.20
LAC800:4	84.9	0.41	14.69	0.0048	0.13
LAC900:4	92.6	0.36	7.04	0.0039	0.06

Supporting Table S2. Ion size, ionic mobility and conductivity of aqueous electrolytes used in electrochemical studies.

	Viscosity (cP)	ions	Conductivity ($cm^2/\Omega mol$)	hydrate ionic radius (Å)
2 M H_2SO_4	1.09[1]	H^+	349.8[2,3]	2.8[3]
		SO_4^{2-}	78.9[3]	3.8[3,4]
2 M KCl	0.91[5]	K^+	73.5[3,6]	2.8-3.31[6-9]
		Cl^-	76.35[2]	3.8[10]

References

1. G. W. Vinal, Craig, D.N., *J. Research*, 1933, **10**, 781-793.
2. M. Berowitz and W. Wan, *J. Chem. Phys*., 1987, **86**, 376-382.
3. X. Zhang, X. Wang, L. Jiang, H. Wu, C. Wu and J. Su, *J. Power Sources*, 2012, **216**, 290-296.
4. E. Frackowiak, Beguin, Francois, ed., *Supercapacitors: materials, systems and applications*, John Wiley & Sons, 2013.
5. J. Kestin, H. E. Khalifa and R. J. Correia, *J. phys. Chem. Ref. Data*, 1981, **10**.
6. R. N. Reddy and R. G. Reddy, *J. Power Sources*, 2003, **124**, 330-337.
7. I. Persson, *Pure Appl. Chem.*, 2010, **82**, 1901-1917.
8. J. Mähler and I. Persson, *Inorg. Chem.*, 2011, **51**, 425-438.
9. M. Inagaki, H. Konno and O. Tanaike, *J. Power Sources*, 2010, **195**, 7880-7903.
10. L. A. Richards, A. Schaefer, B. S. Richards and B. Corry, *Small GTPases*, 2012, **8**, 1701-1709.

Supporting Table S3. A summary of electrolyte properties; molecular weight, electrical conductivity and viscosity of two ionic liquid electrolytes.

	Ionic size (Å)	**Density[a] (g/cm³)**	**Conductivity[b] (mS/cm)**	**Viscosity (cP)[c]**
$[EMIm][EtSO_4]$	(+) 7.8 x 5.8 x 3.3[1]	1.243[3]	3.82[2]	107.7[3] (24 °C) 78.5 (30 °C)
$[BMIm][BF_4]$	(+) 9.7 x 7.0 x 3.3[1] (-) 3.1 x 3.1 x 3.1[1]	1.205[3]	4.38[2]	109.2[3] (20 °C) 75.4 (30 °C)

a The density at 20 °C, *b* the conductivity at 25 °C, *c* 1 cP = 1 m Pa S

References

1. S. Liu, W. Liu, Y. Liu, J.-H. Lin, X. Zhou, M. J. Janik, R. H. Colby and Q. Zhang, *Polym. Int.*, 2010, **59**, 321-328.
2. J. Vila, L. M. Varela and O. Cabeza, *Electrochimica Acta*, 2007, **52**, 7413-7417.
3. J. Jacquemin, P. Husson, A. A. H. Padua and V. Majer, *Green Chem.*, 2006, **8**, 172-180.

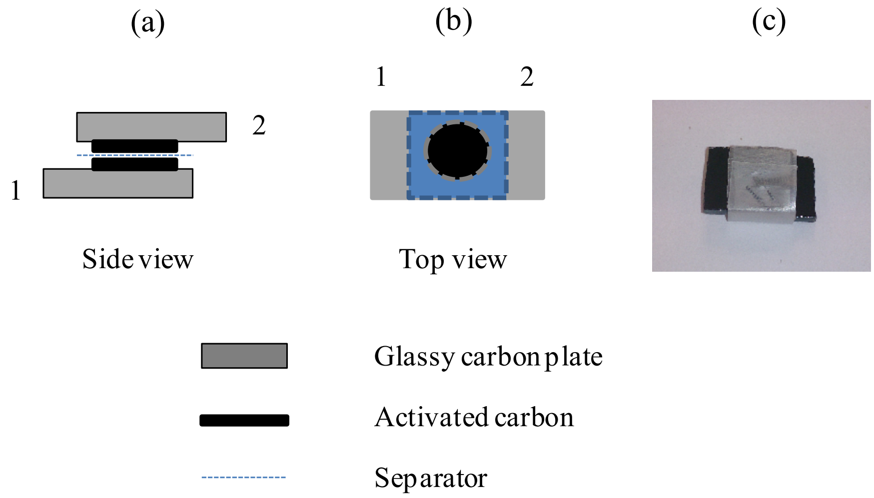

Supporting Figure S1. Schematic of home-made sandwich type electrode (a, b), and an actual electrode image (c).

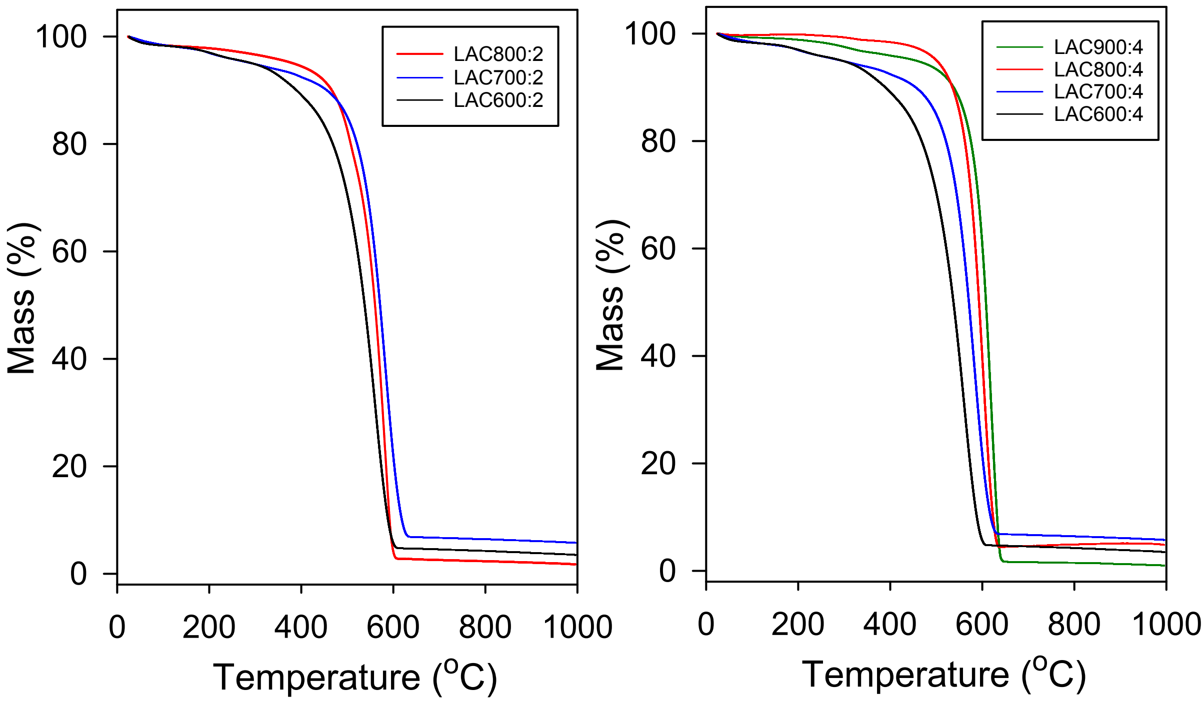

Supporting Figure S2. Thermogravimetric analysis curves of lignin-derived activated carbons; LACT:2 set (left panel) and LACT:4 set (right panel).

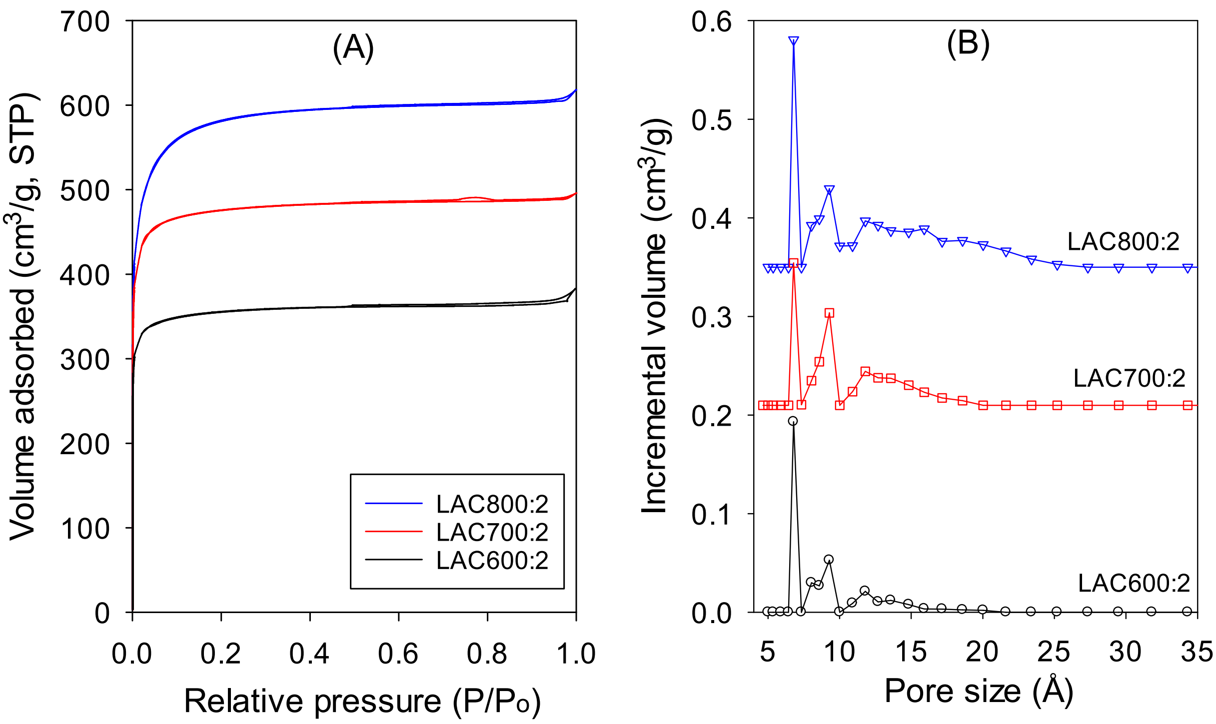

Supporting Figure S3. (A) Nitrogen sorption isotherms and (B) pore size distribution curves of lignin-derived carbon activated at 600 – 800 ^{o}C and KOH/hydrochar ratio of 2.

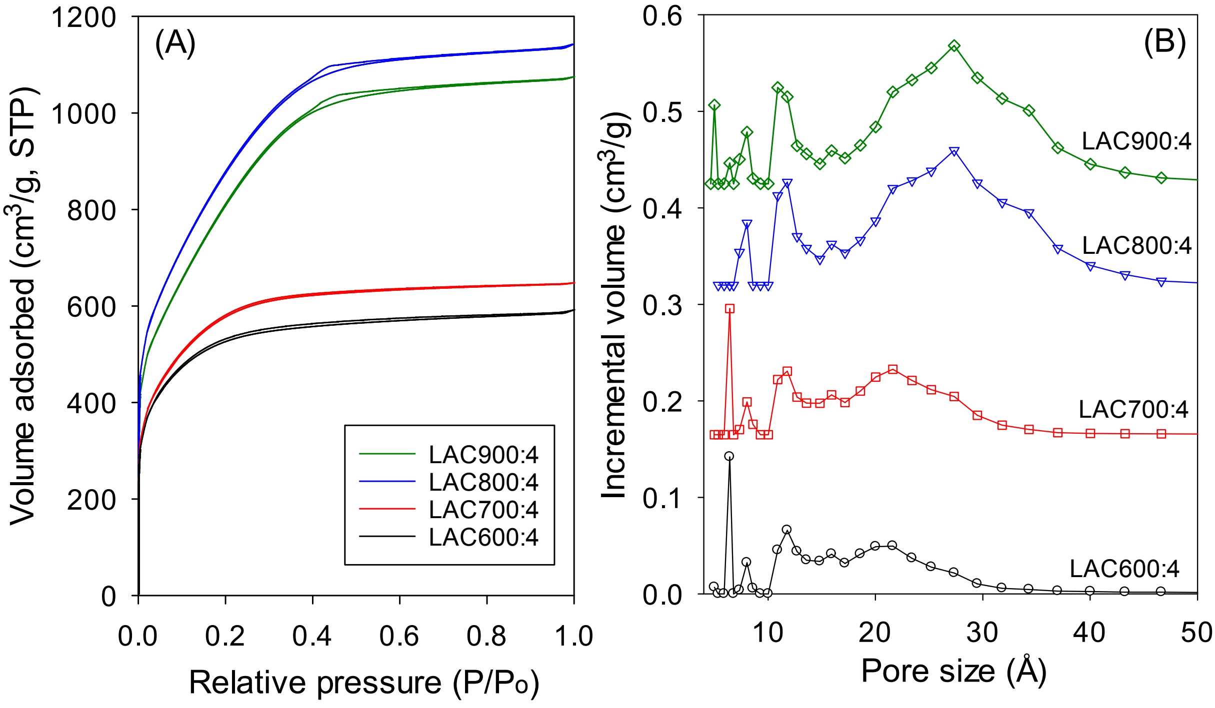

Supporting Figure S4. (A) Nitrogen sorption isotherms and (B) pore size distribution curves of lignin-derived carbon activated at 600 – 900 °C and KOH/hydrochar ratio of 4.

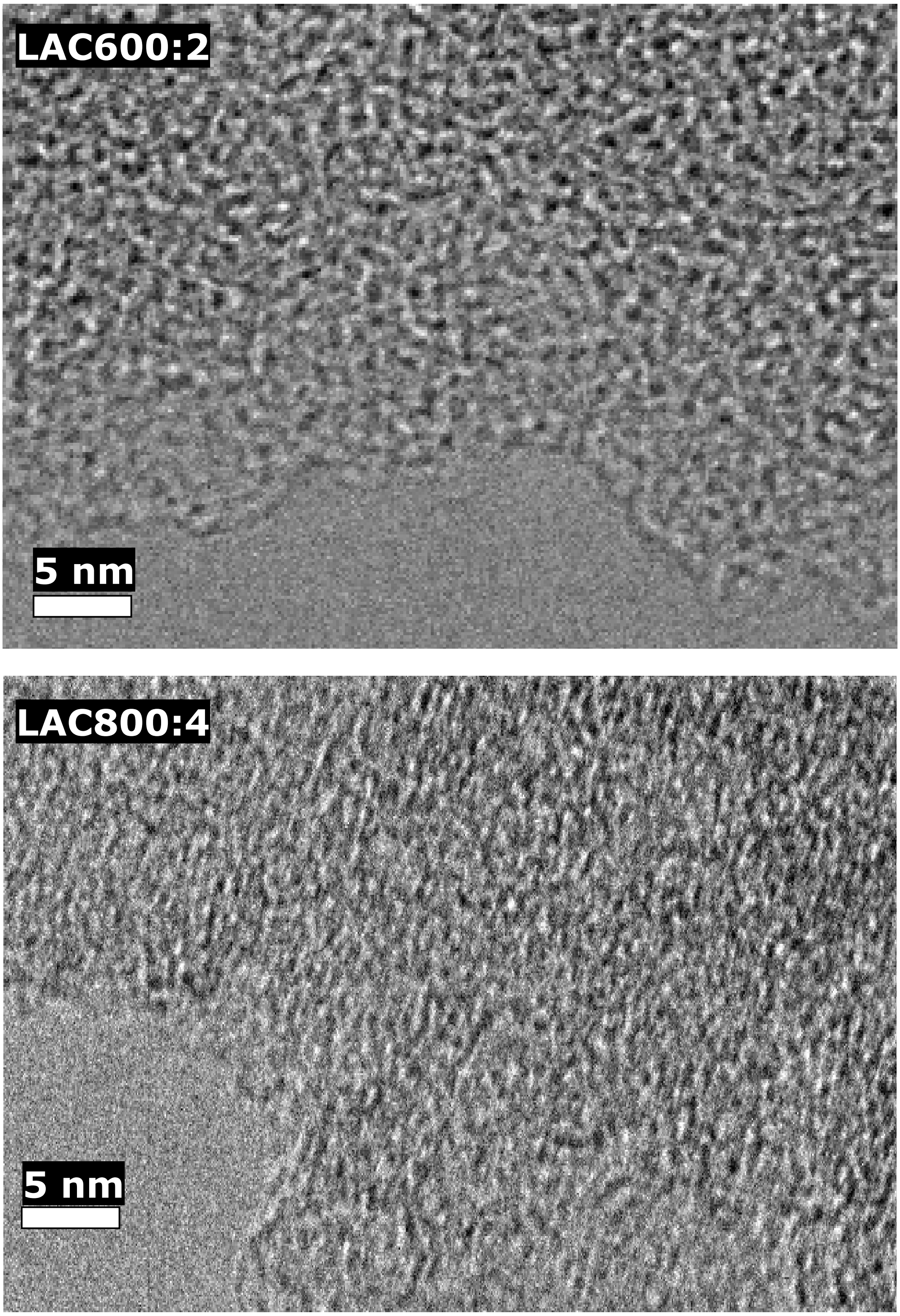

Supporting Figure S5. TEM images of lignin-derived activated carbons.

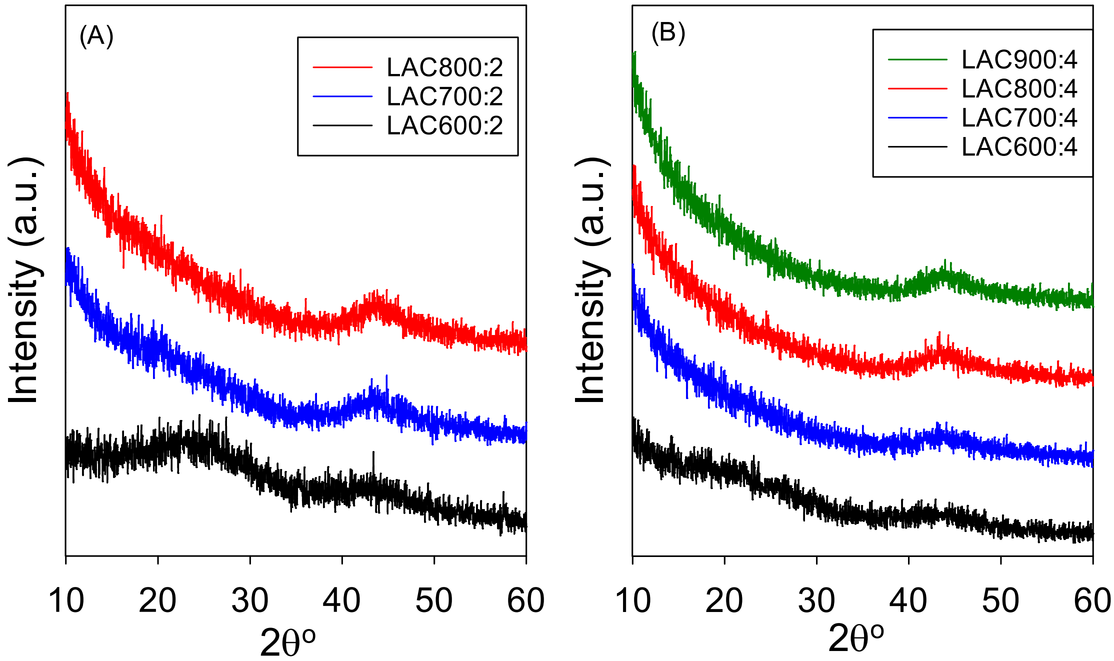

Supporting Figure S6. Powder XRD patterns of lignin-derived carbon activated at 600 – 900 °C and KOH/hydrochar ratio of (A) 2 or (B) 4.

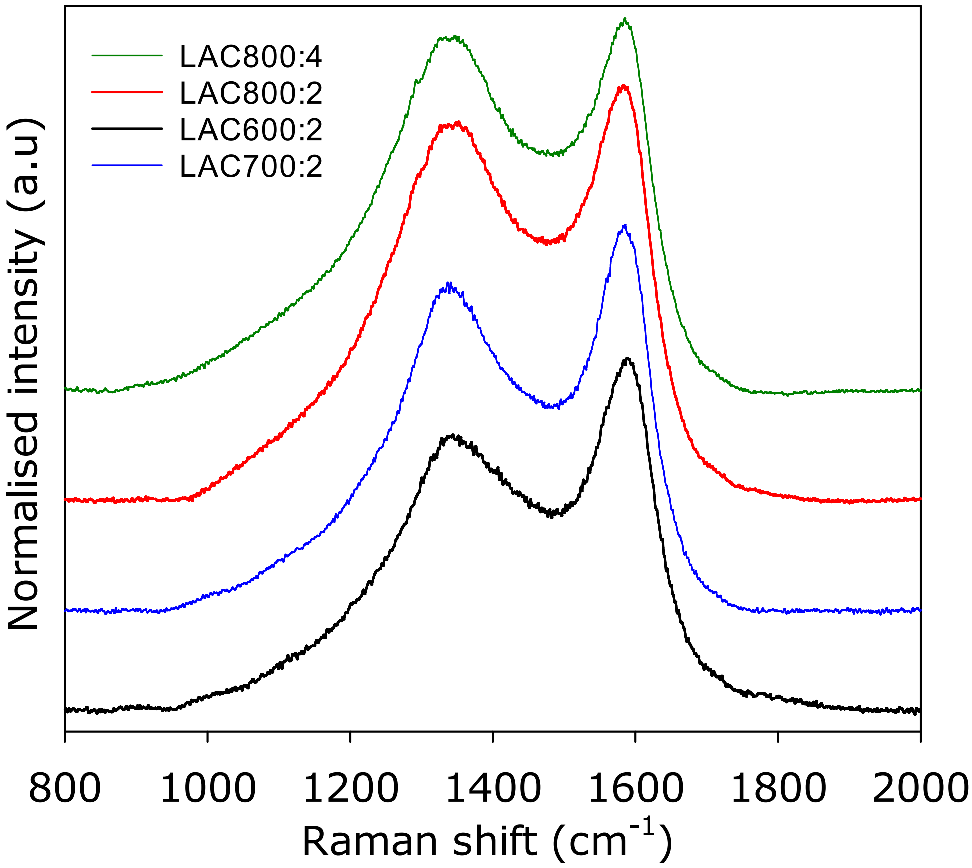

Supporting Figure S7. Raman spectra of lignin-derived activated carbons.

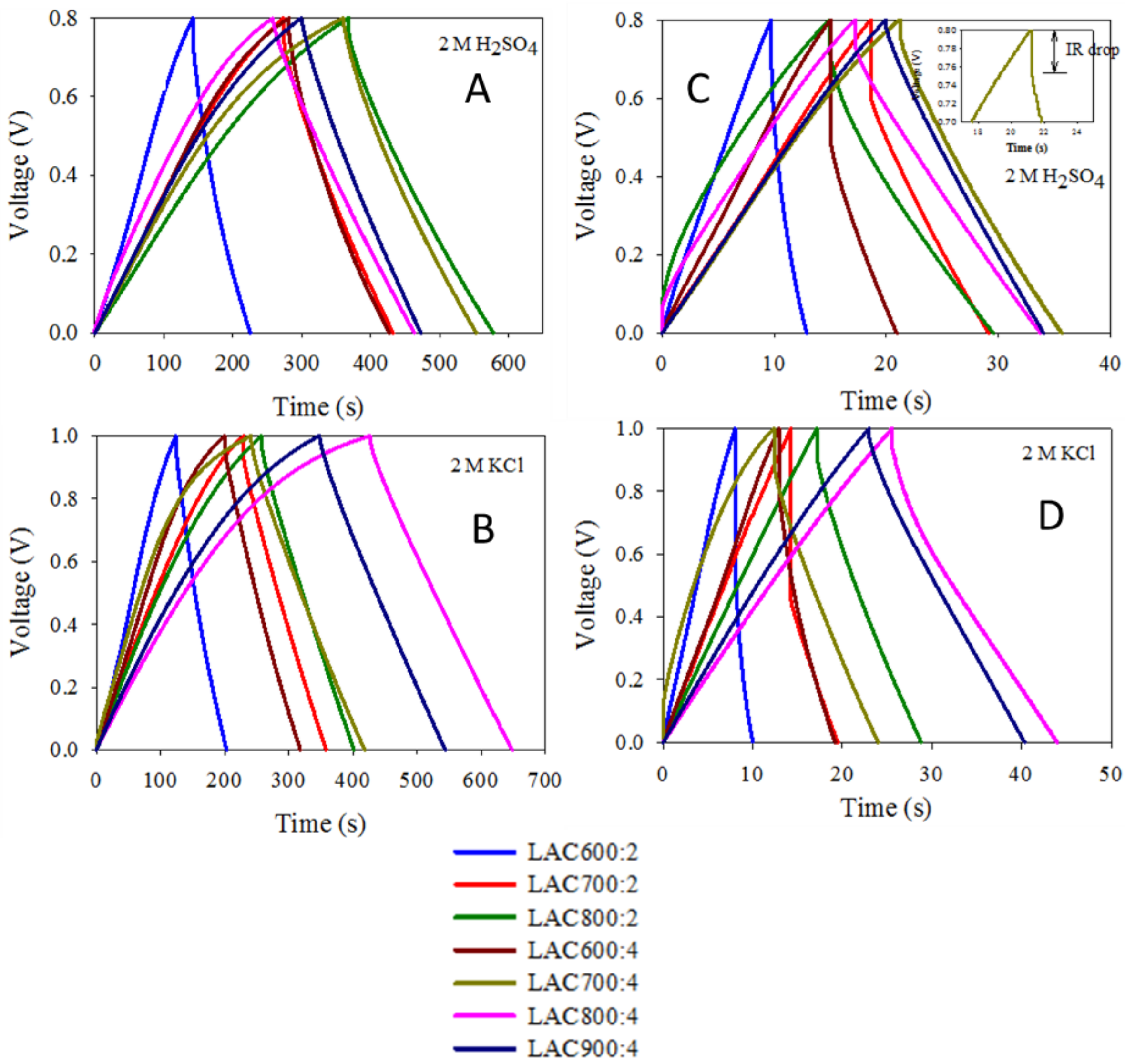

Supporting Figure S8. Galvanostaic charge/discharge curves of all LAC electrodes measured at different current load of 0.5 (A, B) and 5.0 A/g (C, D) in aqueous electrolytes. When the current load increases, a broad IR drop is observed at higher current load of 5 A/g (inset panel C)

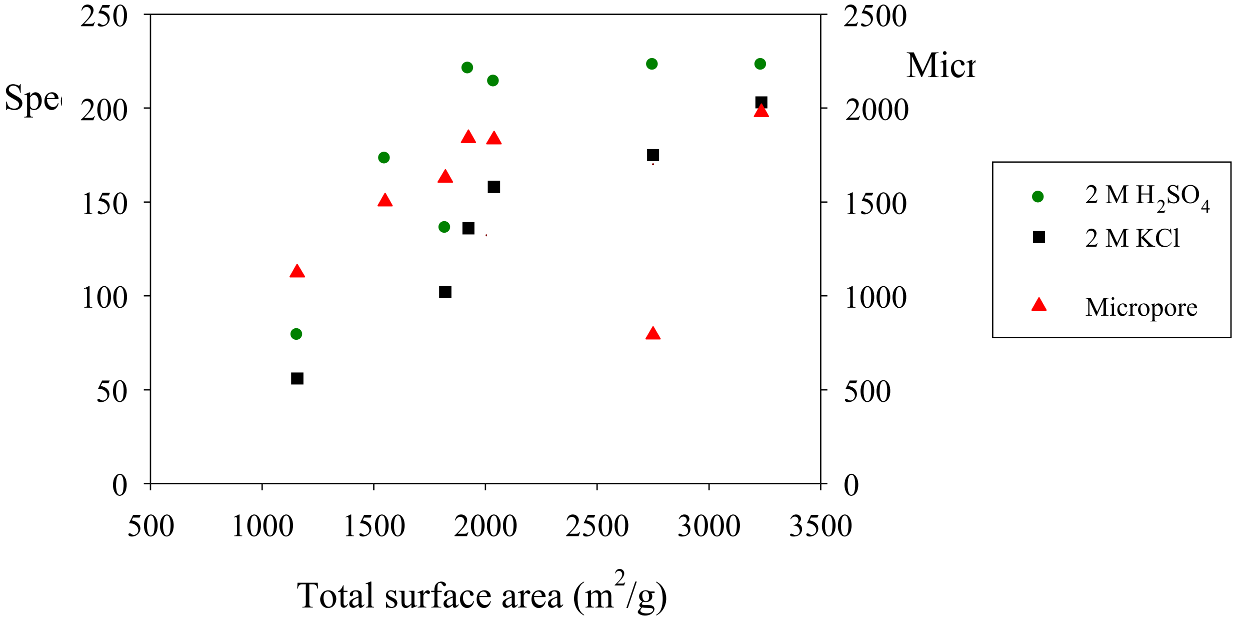

Supporting Figure S9. A plot of specific capacitance and micropore surface area as a function of total surface area of LAC electrodes in three aqueous electrolytes.

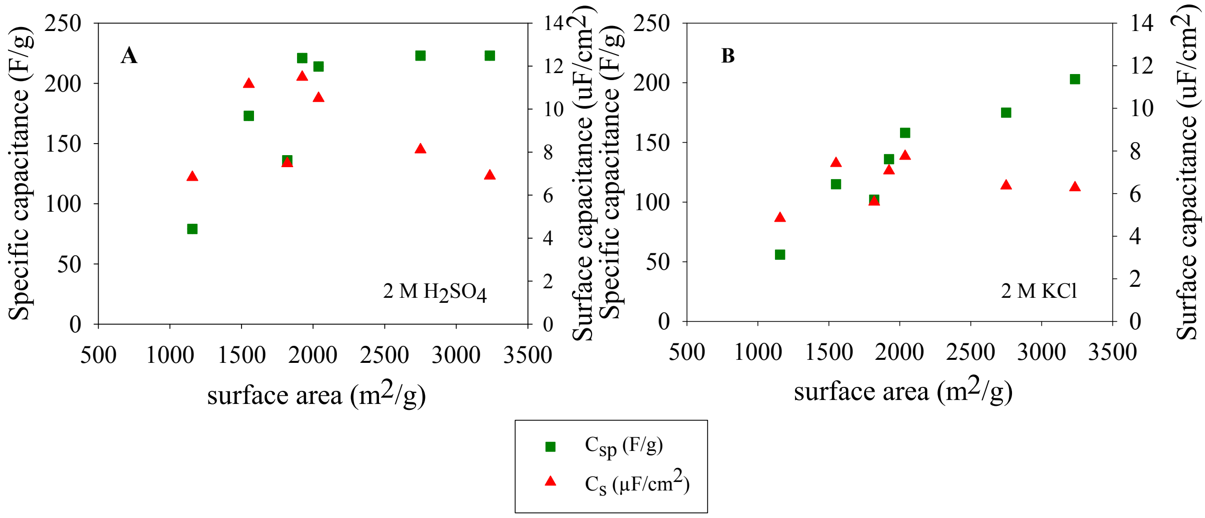

Supporting Figure S10. The correlation between specific capacitance (C_{sp}) and surface area or surface capacitance (C_s) and surface area for LAC electrodes measured in (A) 2 M H_2SO_4, and (B) 2 M KCl electrolyte.

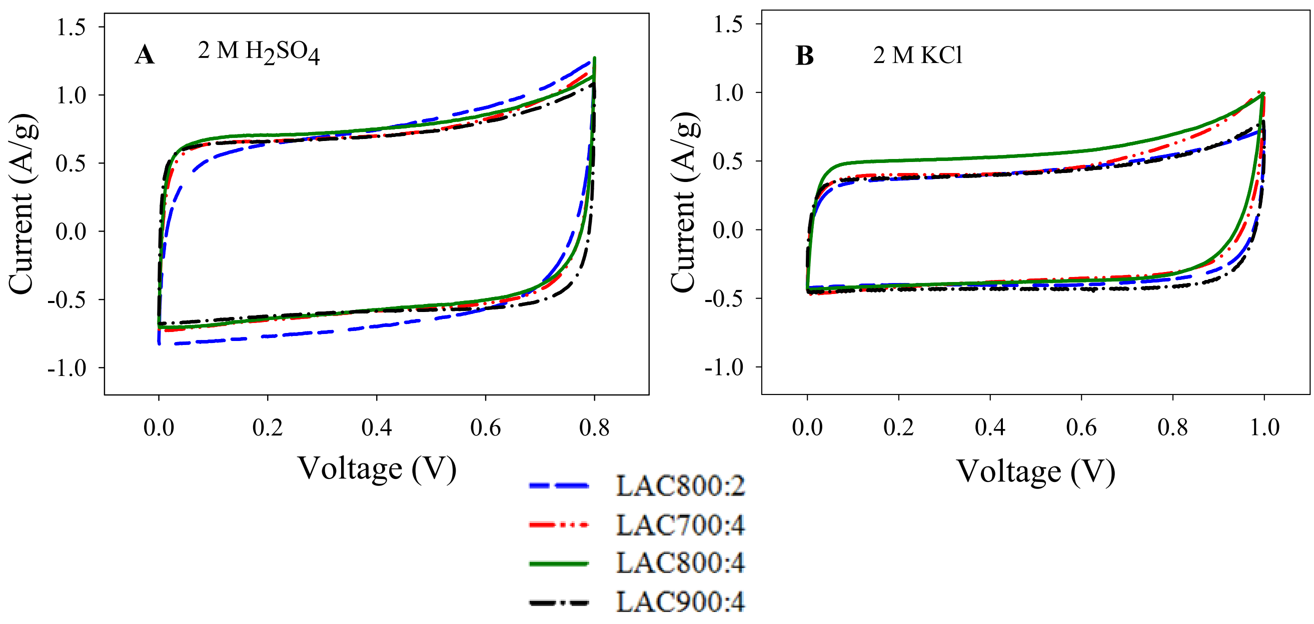

Supporting Figure S11. Cyclic voltammograms of highly porous LAC electrodes at scan rate of 5 mV/s in: (A) 2 M H_2SO_4, and (B) 2 M KCl.

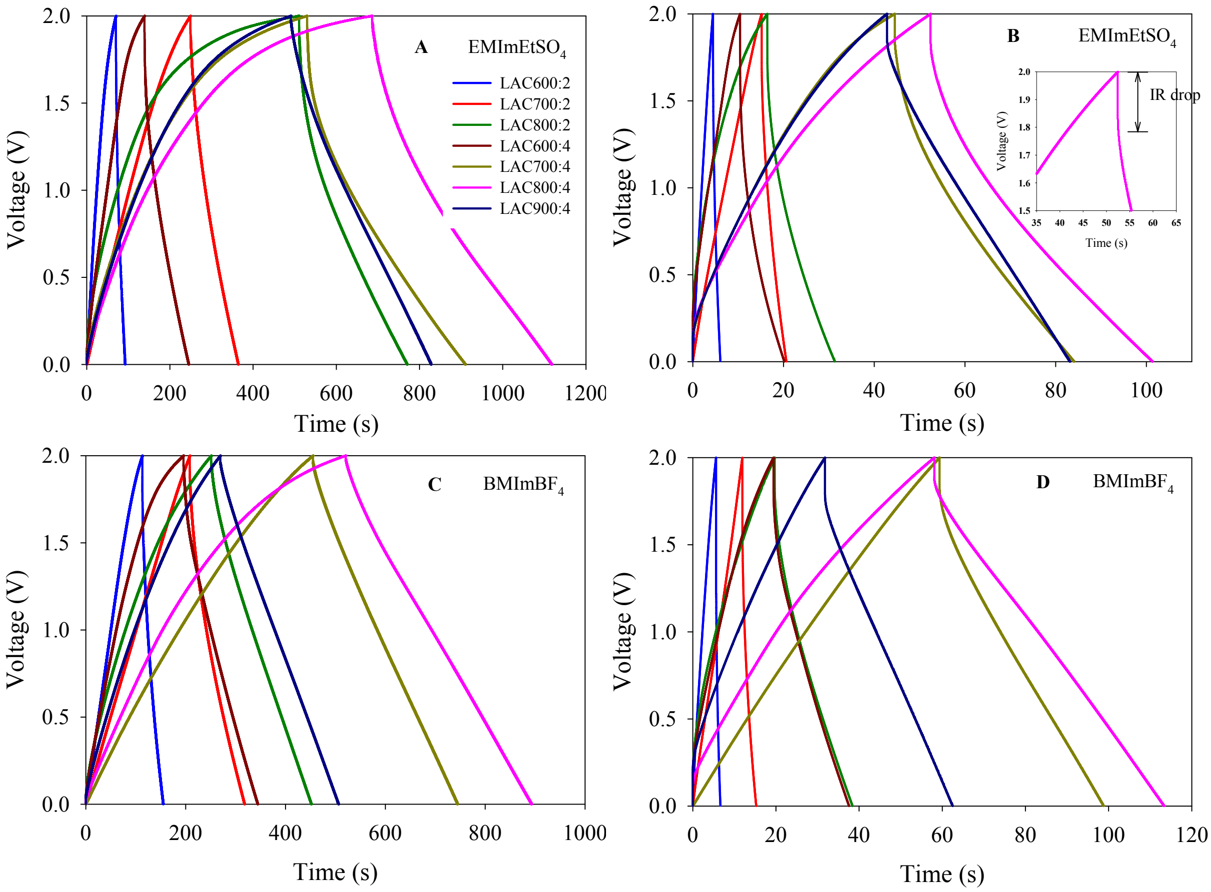

Supporting Figure S12. Galvanostatic charge/discharge curves measured at current load of 0.5 (A, B) and 3.0 A/g (C, D) in $EMImEtSO_4$ and $BMImBF_4$ electrolytes.

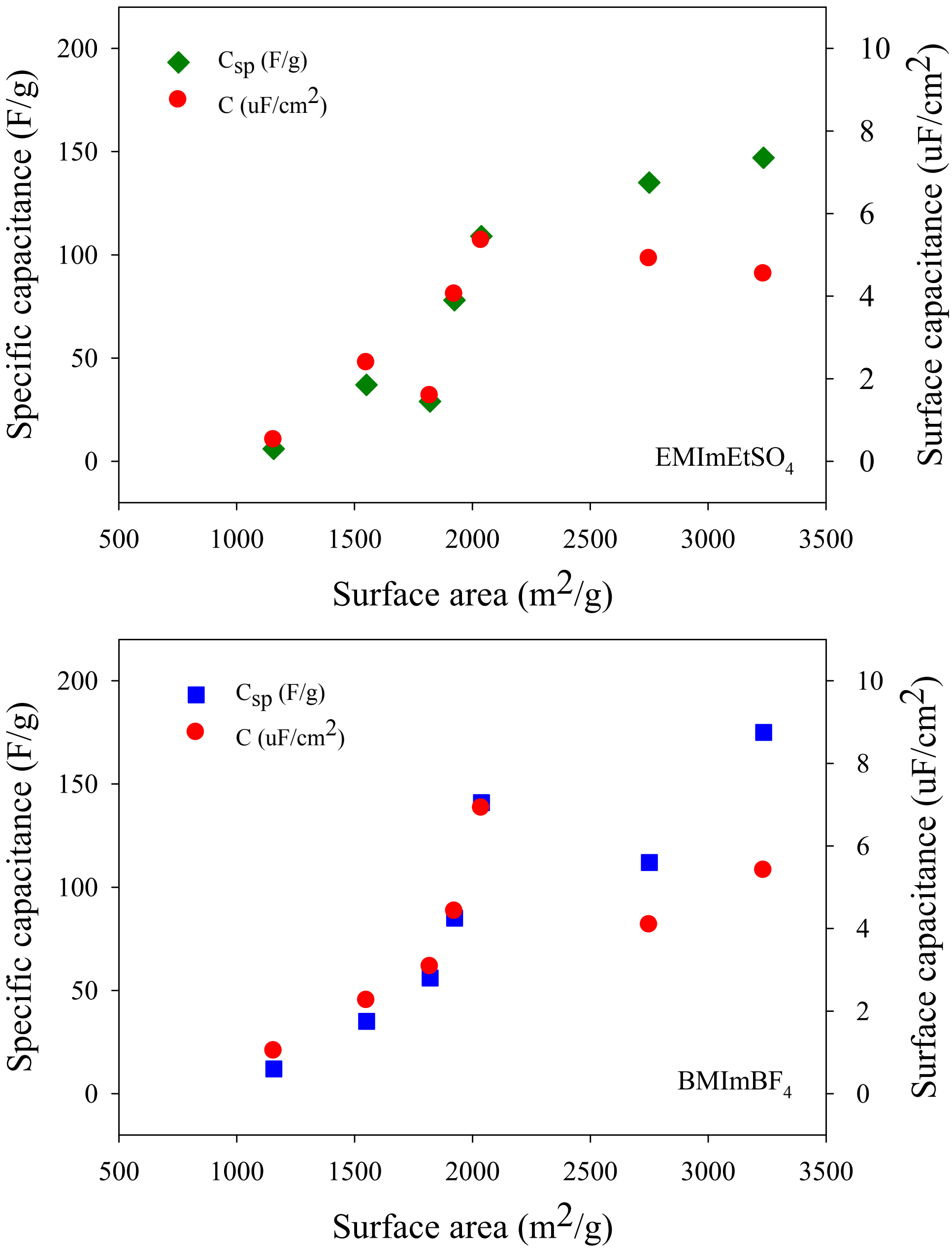

Supporting Figure S13. The relationship between specific capacitance or accessible surface area in term of surface capacitance with surface area of LAC electrodes measured in $EMImEtSO_4$ and $BMImBF_4$ electrolytes.

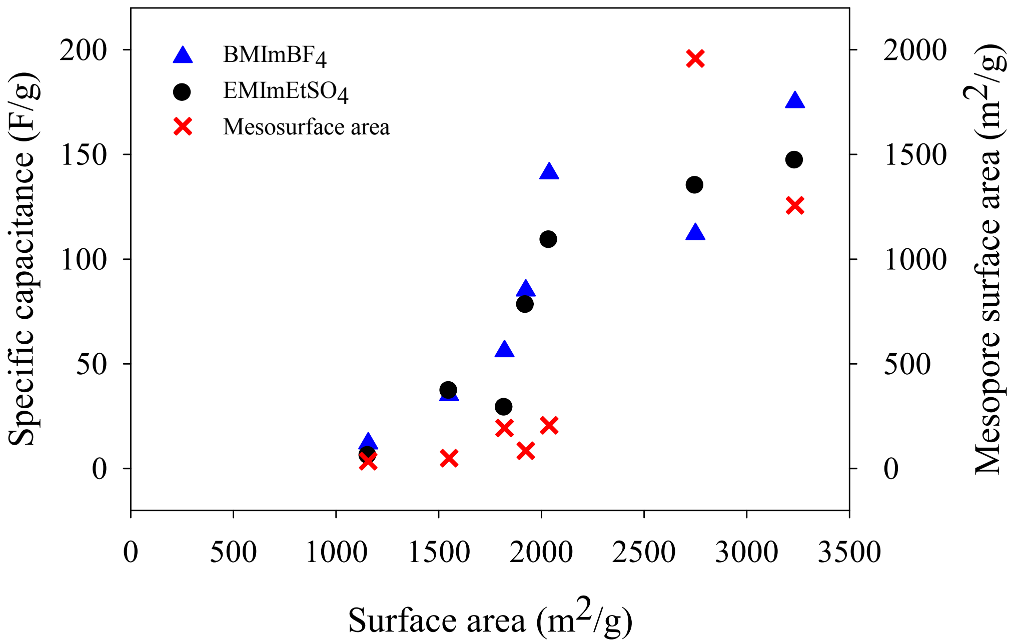

Supporting Figure S14. The correlation between specific capacitance and surface area or mesopores surface area of LAC electrodes measured in $EMImEtSO_4$ and BMImBF4 electrolytes.

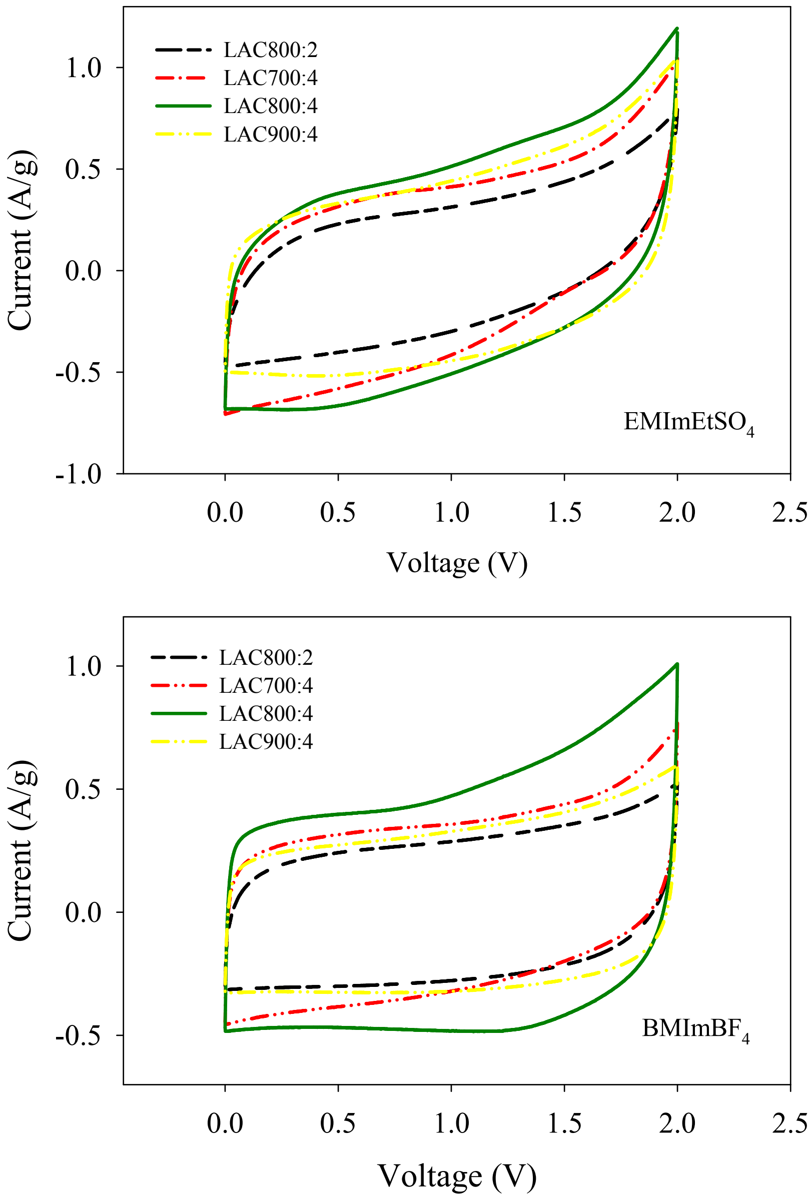

Supporting Figure S15. CV curves of LAC electrodes measured at scan rate of 5 mV/s in two ionic liquid electrolytes; (a) $EMImEtSO_4$, and (b) $BMImBF_4$.